NANO LETTERS

Letter

pubs.acs.org/NanoLett

Surface-Dominated Conduction in a 6 nm thick Bi_2Se_3 Thin Film

Liang He,*[,†,#] Faxian Xiu,[‡,#] Xinxin Yu,[†] Marcus Teague,[∥] Wanjun, Jiang,[†] Yabin Fan,[†] Xufeng Kou,[†] Murong Lang,[†] Yong Wang,[§] Guan Huang,[†] Nai-Chang Yeh,[∥] and Kang L. Wang*[,†]

[†]Device Research Laboratory, Department of Electrical Engineering, University of California, Los Angeles, California 90095, United States

[‡]Department of Electrical and Computer Engineering, Iowa State University, Ames, Iowa 50011, United States

[§]State Key Laboratory of Silicon Materials and Center for Electron Microscopy, Department of Materials Science and Engineering, Zhejiang University, Hangzhou, 310027, China

[∥]Department of Physics, California Institute of Technology, Pasadena, California 91125, United States

ABSTRACT: We report a direct observation of surface dominated conduction in an intrinsic Bi_2Se_3 thin film with a thickness of six quintuple layers grown on lattice-matched CdS (0001) substrates by molecular beam epitaxy. Shubnikov-de Haas oscillations from the topological surface states suggest that the Fermi level falls inside the bulk band gap and is 53 ± 5 meV above the Dirac point, which is in agreement with 70 ± 20 meV obtained from scanning tunneling spectroscopies. Our results demonstrate a great potential of producing genuine topological insulator devices using Dirac Fermions of the surface states, when the film thickness is pushed to nanometer range.

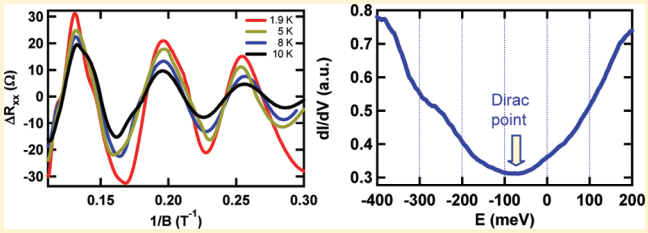

KEYWORDS: *Intrinsic topological insulator, Bi_2Se_3, transport properties, surface states, quantum oscillations*

Three-dimensional (3D) topological insulators (TIs) have attracted great attention from both theoretical and experimental aspects.[1−6] It is known that they have a semiconductor gap in the bulk with an odd number of Dirac-cone surface states. Soon after theoretical predictions, the surface states of 3D TIs have been demonstrated by angle-resolved photoemission spectroscopy (ARPES)[7−10] and scanning tunneling microscopy (STM).[9,11,12] However, a direct transport measurement of the surface effects is significantly hindered by the dominant bulk carrier conduction. Scientist have tried various approaches to overcome the bulk conduction, such as electrical tuning of the Fermi level into bulk band,[13,14] counter doping with Ca or Na,[15] and synthesizing novel complex materials such as $(BiSb)_2Se_3$,[16] and $Bi_2(SeTe)_3$.[17,18] To some extent, these approaches have demonstrated success in enhancing surface conduction. However, the fundamental understanding of surface conduction in high quality samples is crucial for utilization of surface states in microelectronics and spintronics. In this paper, we report high-crystalline quality Bi_2Se_3 thin films grown on CdS (0001) substrate by molecular beam epitaxy demonstrate surface-dominated conduction. Importantly, the Fermi levels of current thin films fall inside the bulk band gap. As a result, the surface-state conduction can be clearly distinguished from other conducting channels. In particular, for a 6 quintuple layers (QLs) thin film, we show most of conduction come from the surface.

Bi_2Se_3 thin films were grown within an ultrahigh vacuum MBE chamber on lattice-matched insulating CdS (0001).[19] After growth, standard Hall bar devices were fabricated with a physical mask, as shown schematically in Figure 1a. The longitudinal sheet resistance (R_s) as a function of temperature (T) is displayed in Figure 1b, where four different regimes can be clearly identified, marked as I, II, III, and IV from high to low temperatures. In regime I, for thinner films (<9 QLs) R_s exponentially increases as the temperature decreases. This is most likely associated with the bulk band gap. The activation energy of it can be estimated from the Arrhenius slope of $\ln(R_s)$ versus $1/T$.[20,21] The thickness dependent activation energy is plotted in Figure 1c. The systematic increase of the estimated bulk band gap with reducing the film thickness is attributed to the quantum confinement of the film along the growth direction (perpendicular to the substrate), which is qualitatively agreed with the recent ARPES measurements of Bi_2Se_3 grown on SiC (0001) by MBE.[22] For thicker films, however, R_s does not show the same exponential behavior at high temperatures, which can be ascribed to the overwhelming electrons activated from the bulk impurity band as will be discussed later.

In Regime II, the resistance reduces as temperature decreases, resembling a metallic behavior as observed widely in TIs.[13,16,23, 24] Such a decrease can be explained by alleviated phonon scatterings when temperature decreases. This can be further confirmed by a power-law increase of mobility ($\mu \propto T^{-2}$), as will be described in Figure 2e (dashed line). In Regime III (30 K < T < ∼80 K), the resistivity exhibits another

Received: December 1, 2011
Revised: February 1, 2012
Published: February 8, 2012

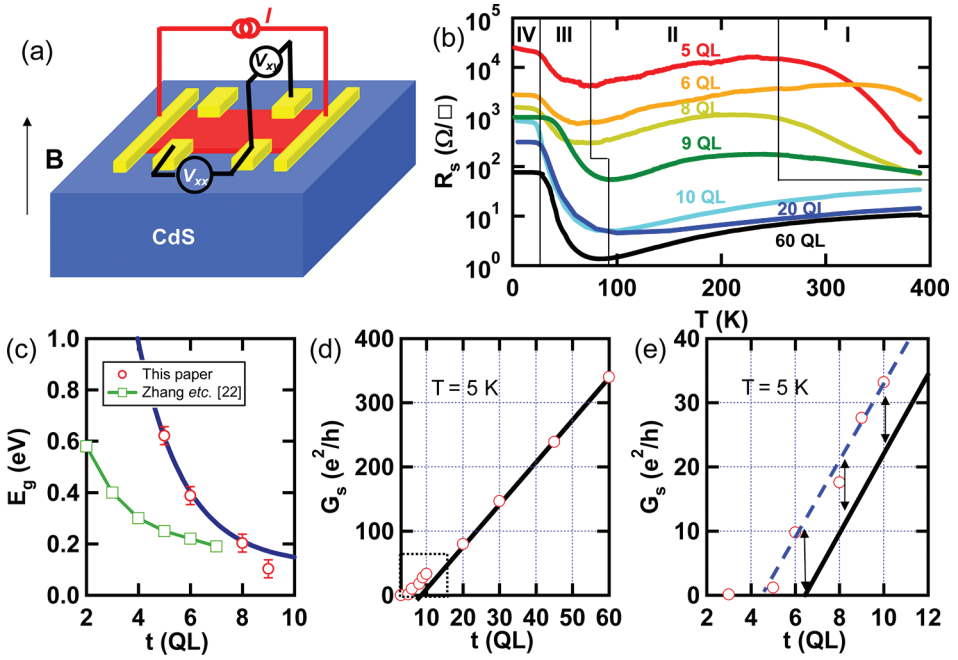

Figure 1. (a) Schematic diagram of a typical Hall bar sample. The channel size is 8 mm × 1 mm. A constant current geometry was used for transport measurement. (b) Temperature dependent sheet resistance R_s (R_{xx}) of films ranging from 5 to 60 QLs. (c) Estimated bulk band gap vs film thickness. (d) Total conductance vs film thickness at 5 K. The solid line presents a linear fit for the four thicker films (20−60 QLs), exhibiting a thickness dependence of impurity band conduction and enabling the determination of a critical thickness of 6.4 QL (intercepting the abscissa), below which surface states is the only conducting channel at low temperature. (e) Expanded plot for the thin film range of (d), dotted square. The solid line is the same solid line in (d). The dashed line is the fitted data for thin layer samples. The difference representing the surface conduction fit to 6.4 QL sample is ∼10 e^2/h.

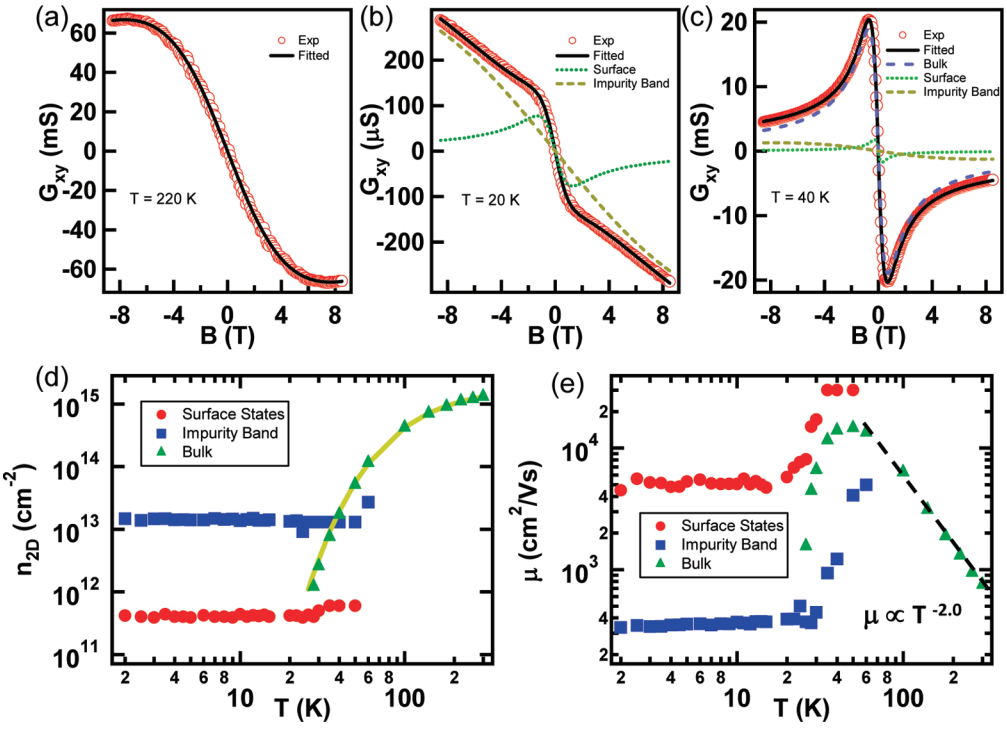

Figure 2. Hall conductance of a 10 QL sample, from which transport properties of three channels: the bulk, the impurity band, and the surface states at various temperatures have been extracted. Magnetic field dependent G_{xy} at various temperatures of (a) 220 K, (b) 20 K, and (c) 40 K. Open circles are experimental data and solid lines are fitted results (d) 2D carrier density vs temperature. Solid yellow line represents the Fermi−Dirac distribution of the bulk carrier density equivalent to 2D. (e) Mobility vs temperature for the three channels. Dashed line represents the power low dependence of $\mu \propto T^{-2}$, which suggests the mechanism of phonon scattering in these temperatures.

exponential increase with respect to $1/T$. This exponential increase is most likely associated with the frozen-out effect of electrons from the bulk conduction band to a shallow impurity band below it.[21,25] In Regime IV (T < 30 K), the resistivities of

dx.doi.org/10.1021/nl204234j | Nano Lett. 2012, 12, 1486−1490

all samples approach to constant values. A similar temperature-dependent behavior was reported in our previous work: Bi_2Se_3 grown on Si (111) substrate.[26] And this temperature regime is believed to be dominated by surface conduction.

In Region IV where the bulk carriers freeze out, the transport is presumably a combination of surface states and impurity band conduction.[17,18,21] The sheet conductance is monotonically increases with film thickness as shown in Figure 1d. This variation of the conductance with film thickness is attributed to the impurity band. By fitting the conductance of thicker films (20−60 QLs), where the impurity band conduction dominates, a linear relationship of $G = 8.75 \times (t\text{-}6.4)$ can be obtained (solid line in Figure 1d,e), where G is the conductance in the unit of e^2/h, and t is the film thickness. This result suggests that below a critical thickness of 6.4 QLs, the contribution from the thickness dependent component is close to zero.

We have noticed linearly fitted solid line from the thicker samples deviated from the data of thinner films below 10 QLs, as shown in Figure 1e. The difference of ∼10 e^2/h, as indicated by the double arrows, is considered to be the conduction from the surface states which agrees closely with the Hall data to be described later. As samples getting thinner, the surface states also open a band gap because of the hybridization between the top and bottom surfaces;[22] therefore the metallic surface states seem to disappear. These samples behave like normal insulators and thus the conductance drops dramatically down to 1.5 e^2/h (5 QLs) and 0.1 e^2/h (3 QLs). On the basis of the simplified model, for samples around the critical thickness (∼6.4 QLs), the surface state conduction is the dominant channel. In other words, for our 6 QL sample, most of the total conduction is provided by surface states.

In order to further investigate the multiple channel conduction for thicker films, magnetic field and temperature dependent longitudinal resistance (R_{xx}) and Hall resistance (R_{xy}) have been measured. These data reveal the coexistence of three conducting channels: the bulk, the impurity band and the surface states.[17] The parallel Hall conductance is given by

$$G_{xy} \equiv \frac{R_{xy}}{R_{xy}^2 + R_S^2} = G_{\mathrm{Bulk}} + G_{\mathrm{Impurity}} + G_{\mathrm{Surface}} \quad (1)$$

where R_{xy} is the Hall resistance, R_s is the sheet resistance, G_{Bulk}, G_{impurity}, and G_{surface} represent the Hall conductance of the bulk, the impurity band, and the surface states, respectively. Additionally, the Hall conductance of each channel is described by a semiclassical expression

$$G = en\mu\frac{\mu B}{(1 + \mu^2 B^2)} \quad (2)$$

where n is the 2D carrier density and μ is the mobility of each channel.[16] As an example, we present the analysis results of the Hall conductance for a 10 QL sample at different temperatures as described below.

At high temperatures (Regime II in Figure 1b) where the phonon scattering dominates, the total conductance is then overwhelmed by electrons in the bulk conduction band excited from the impurity band. As a result, the total conductance of G_{xy} can be simplified by the dominant bulk conducting channel, as given in Figure 2a. At low-temperature (Regime IV in Figure 1b), when all electrons are frozen in the impurity band, there is nearly no contribution from bulk, thus the total conduction is a combination of those of the surface and the impurity band, evident in Figure 2b. In the intermediate temperature (Regime III in Figure 1b), the total conduction consequently results from all three channels, illustrated in Figure 2c. Following this procedure, we can obtain the temperature dependence of carrier density and mobility for the three channels (1.9−300 K).

Figure 2d illustrates the temperature dependence of the two-dimensional carrier density of the three channels. The bulk carrier densities (green triangles) decrease exponentially as carriers are frozen to the impurity band. Since the carriers in the bulk conduction band are electrons, their temperature dependent density can be described as a classic Fermi-Dirac distribution of $n_b = n_0/(e^{E_a/k_BT} + 1)$ (solid yellow line in Figure 2d), where n_0 is the bulk carrier density of $\sim 4 \times 10^{15}$ cm^{-2}, and E_a of 20 meV is the energy gap between the impurity band and the bottom of the bulk conduction band. The carrier densities of the impurity band (blue squares) and surface states (red circles) remain approximately a constant of 1.3×10^{13} and 4×10^{11} cm^{-2}, respectively. Figure 2e shows the corresponding mobility at different temperatures. The mobilities of bulk electrons (green triangles) exhibits a power law $\mu \propto T^{-2}$ at high temperatures, consistent with the dominant phonon scattering as mentioned before in the Region II of Figure 1b. At low temperatures ($T < 20$ K), mobilities of both the impurity band and the surface states reach constant values of ∼380 and ∼5000 $cm^2\ V^{-1}\ s^{-1}$, respectively. On the basis of the above analysis, we can subsequently estimate the longitudinal conductance G_{xx} (= *neu*) of 20 and 8 e^2/h for the impurity band and the surface states, respectively. The numbers are in quantitative agreement with the previous results from the thickness dependent conductance as shown in Figure 1e, in which the estimated conductance of the impurity band and surface states is 22 and 10 e^2/h, respectively, for 10 QL sample.

As we demonstrated above, samples with a film thickness around 6.4 QLs will have the most pronounced surface conduction. Indeed, we have observed characteristic quantum oscillations originated from the surface states for our 6 QL sample. In Figure 3a, we present the field dependent longitudinal resistance, R_{xx}, acquired at 1.9 K for the 6 QL sample. Strong oscillations of R_{xx} at various temperatures after subtracting a smooth background can be observed, as shown in Figure 3b. The oscillations become stronger with the increase of magnetic field and decrease of temperature. For a two-dimensional Fermi surface, the peak positions depend only on the field $B_\perp = B\cos(\theta)$, normal to sample surface, (θ is the tilt angle between B and c axis). As show in the inset of Figure 3b, the peak field of Landau level $n = 3.5$ (second peak in Figure 3a) has been plotted at different field angels. It follows $1/\cos(\theta)$ perfectly, suggesting the SdH oscillations originated from a 2D Fermi surface. It is well know that in the SdH oscillations, the Landau level index n is related to the cross section area of the Fermi surface (S_F) by

$$2\pi(n + \gamma) = S_F\frac{\hbar}{eB} \quad (3)$$

where e is the electron charge, $\hbar$ is the Plank's constant divided by 2π, B is the magnetic flux density, and $\gamma = 1/2$ or 0 represents the Berry phase of π or 0. As shown in Figure 3c, the value of $1/B$ corresponding to the maximum and the minimum in ΔR_{xx} (arrows in Figure 3a) is plotted as a function of the Landau-level number. A linear fit yields $S_F = 1.53 \times 10^{17}$ m^{-2} with the Fermi wave vector $k_F = 0.022$ $Å^{-1}$, and a 2D carrier density of 3.9×10^{11} cm^{-2}, consistent with our previous results of 4×10^{11} cm^{-2} for the surface states in

dx.doi.org/10.1021/nl204234j | Nano Lett. 2012, 12, 1486−1490

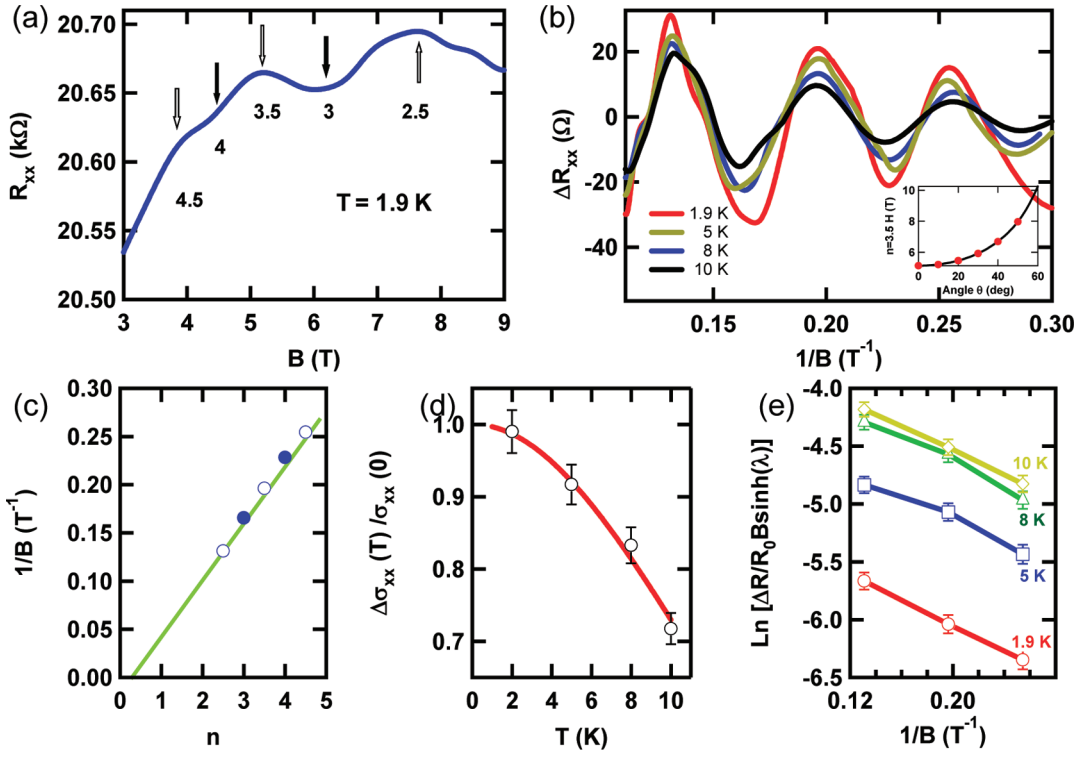

Figure 3. Shubnikov-de Haas oscillations of the surface states of a 6 QL sample. (a) Longitudinal resistance R_{xx} vs magnetic field at T = 1.9 K. Solid arrows indicate the integer Landau levels from the valley values; open arrows give the peak values. (b) ΔR_{xx} vs $1/B$ at different temperatures. The insert shows the field position of the n = 3.5 LL peak varies with θ as $1/\cos\theta$ (solid black line), suggesting a 2D Fermi surface. (c) Landau level index plot: $1/B$ vs n. The open (close) circles are the Landau level of the maxima (minima) of ΔR_{xx}. (d) Normalized conductivity amplitude $\Delta\sigma_{xx}(T)/\Delta\sigma_{xx}(0)$ vs temperature (7.6 T). The effective mass deduced is ~0.07 m_e. (e) Dingle plot of $\ln[(\Delta R/R_0)B\sinh(\lambda)]$ vs $1/B$, used to determine τ and l.

Figure 2d. The n-axis intercept, $\gamma \sim 0.35 \pm 0.08$ slightly deviates from exactly π-Berry phase, as has also been reported on other SdH studies of TIs.[17,18,24,27]

Following the Lifshitz–Kosevich (LK) theory,[28] the temperature dependence of the SdH amplitude is described by $\Delta\sigma_{xx}(T)/\Delta\sigma_{xx}(0) = \lambda(T)/\sinh(\lambda(T))$. The thermal factor is given by $\lambda(T) = 2\pi^2 k_B T m_{cyc}/(\hbar e B)$, where m_{cyc} is cyclotron mass and $\hbar$ is the reduced Planck constant. As shown in Figure 3d, the best fit gives the cyclotron mass $m_{cyc} = 0.07\ m_e$, where m_e is the free electron mass. Assuming that the electrons are Dirac type, the Fermi velocity can be calculated as $\nu_F = \hbar k_F/m_{cyc} = 3.6 \times 10^5$ m s^{-1}, and $E_F = m_{cyc}\nu_F^2 = 53$ meV. The estimated Fermi level of 53 meV above the Dirac point is surprisingly low, suggesting the surface carriers are electrons and the E_F is within the bulk band gap.

To acquire the lifetime of the surface states (τ), the Dingle factor e^{-D} has been examined, where $D = 2\pi^2 E_F/(\tau e B V_F^2)$.[13,16] Note that $\Delta R/R$ is proportional to $[\lambda(T)/\sinh(\lambda(T))]e^{-D}$, and the lifetime can be inferred from the slope in the logarithmic plot of $\log[(\Delta R/R_0)B\ \sinh(\lambda(T))] \sim [2\pi^2 E_F/(\tau e V_F^2)](1/B)$ (Figure 3e). By applying the extracted cyclotron mass, the scattering time $\tau = 1.3 \times 10^{-12}$ s can be estimated. Thus the mean-free path of the surface electrons is $l = \nu_F\tau = 4.6 \times 10^{-7}$ m, and the surface mobility is $\mu = (e\tau)/(m_{cyc}) = 13\,200$ $cm^2\ V^{-1}\ s^{-1}$. We have noticed that the estimated mobility is higher than the results from our previous fitting from Hall data of surface carrier mobility, 5000 $cm^2V^{-1}\ s^{-1}$. In other systems,[17,28,29] the similar discrepancy was also observed, and the reason maybe lies in the difference between relaxation time and scattering time.[30]

To investigate the surface states as well as the position of surface Fermi level, we performed ARPES measurements on our samples. Figure 4a presents a standard ARPES spectroscopy cut along Γ–K direction of a 60 QL sample, the zero point of the energy scale has been shifted to the Dirac point. We have noticed that the Fermi level of the ARPES data is inside the bulk conduction band. This may be due to the n-type doping over long time between sample growth and ARPES measurement, as previously show.[18,31] Another possible reason is due to optical doping induced charge accumulation during ARPES measurement.[31] By finding the maximum of the surface state in the K direction for different energies, we can attain the Fermi area and the surface carrier density (n_s) as a function of energy. In Figure 4b, the horizontal axis has been scaled to fit our experiment data (red circle). The green square is adopted from ref 24, and the purple triangles are the results from our other samples of Bi_2Se_3 grown on Si(111).[32] The consistence between transport results and ARPES supports our estimation of the Fermi level position.

Scanning tunneling spectroscopy (dI/dV) was also performed on the 6 QL sample to measure the density of states (DOS). As expected, the minimum of the conductance corresponding to the Dirac point is ~70 ± 20 meV below the Fermi level (Figure 4c), in reasonable agreement with our estimation from the SdH oscillations. The STS data further confirms that our Fermi level is inside the bulk band gap and very close to the Dirac point.

To conclude, we have observed surface dominated conduction from a 6 QL Bi_2Se_3 thin film grown by MBE. We demonstrated that the intrinsic Bi_2Se_3 thin film has a Fermi

dx.doi.org/10.1021/nl204234j | Nano Lett. 2012, 12, 1486–1490

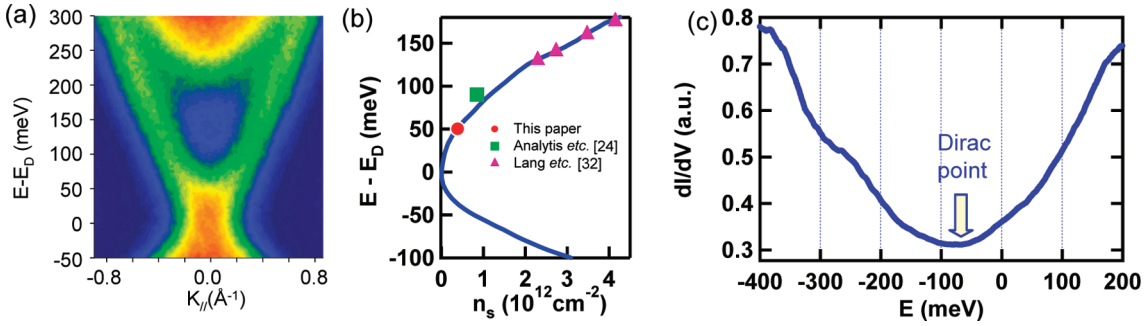

Figure 4. (a) A standard APRES image of a 60 QL sample showing the surface states and the Dirac point. (b) Surface density of states (n_s) vs energy. The data are extracted from ARPES measurement, and horizontal axis has been scaled to fit the transport measurements. The red circle indicates our experiment result in this paper. The green square is adopted from ref 24. The purple triangles are the data from our other samples of Bi_2Se_3 grown on Si(111).[32] (c) Scanning tunneling spectroscopy of a 6 QL sample. Spatially averaged density of states (dI/dV) measurements show the Dirac point is about ~70 ± 20 meV below the Fermi surface.

level positioned within bulk band gap. Our results shed the light on the possibility of producing genuine topological insulator states on lattice-matched CdS substrate and pave a pathway toward the practical device application of topological insulators.

AUTHOR INFORMATION

Corresponding Author

*E-mail: (L.H.) heliang@ee.ucla.com; (K.L.W.) wang@ee.ucla.edu.

Author Contributions

#These authors contributed equally.

Notes

The authors declare no competing financial interest.

ACKNOWLEDGMENTS

This work was in part supported by the Focus Center Research Program - Center on Functional Engineered Nano Architectonics (FENA) and DARPA. Y.W. acknowledges the support from the National Science Foundation of China (No. 11174244).

REFERENCES

(1) Fu, L.; Kane, C. L.; Mele, E. J. *Phys. Rev. Lett.* **2007**, *98* (10), 106803−106803.

(2) Fu, L.; Kane, C. L. *Phys. Rev. B* **2007**, *76* (4), 045302.

(3) Moore, J. E.; Balents, L. *Phys. Rev. B* **2007**, *75*, 121306(R).

(4) Zhang, H.; Liu, C.-X.; Qi, X.-L.; Dai, X.; Fang, Z.; Zhang, S.-C. *Nat. Phys.* **2009**, *5* (6), 438−442.

(5) Moore, J. *Nat. Phys.* **2009**, *5* (6), 378−380.

(6) Franz, M. *Nat. Mater.* **2010**, *9* (7), 536−537.

(7) Hsieh, D.; Qian, D.; Wray, L.; Xia, Y.; Hor, Y. S.; Cava, R. J.; Hasan, M. Z. *Nature* **2008**, *452* (7190), 970−974.

(8) Chen, Y. L.; Analytis, J. G.; Chu, J.-H.; Liu, Z. K.; Mo, S.-K.; Qi, X. L.; Zhang, H. J.; Lu, D. H.; Dai, X.; Fang, Z.; Zhang, S. C.; Fisher, I. R.; Hussain, Z.; Shen, Z.-X. *Science* **2009**, *325* (5937), 178−181.

(9) Hor, Y. S.; Richardella, A.; Roushan, P.; Xia, Y.; Checkelsky, J. G.; Yazdani, A.; Hasan, M. Z.; Ong, N. P.; Cava, R. J. *Phys. Rev. B* **2009**, *79* (19), 195208.

(10) Hsieh, D.; Xia, Y.; Qian, D.; Wray, L.; Meier, F.; Dil, J. H.; Osterwalder, J.; Patthey, L.; Fedorov, A. V.; Lin, H.; Bansil, A.; Grauer, D.; Hor, Y. S.; Cava, R. J.; Hasan, M. Z. *Phys. Rev. Lett.* **2009**, *103* (14), 146401.

(11) Roushan, P.; Seo, J.; Parker, C. V.; Hor, Y. S.; Hsieh, D.; Qian, D.; Richardella, A.; Hasan, M. Z.; Cava, R. J.; Yazdani, A. *Nature* **2009**, *460* (7259), 1106−1109.

(12) Alpichshev, Z.; Analytis, J. G.; Chu, J. H.; Fisher, I. R.; Chen, Y. L.; Shen, Z. X.; Fang, A.; Kapitulnik, A. *Phys. Rev. Lett.* **2010**, *104* (1), 016401.

(13) Xiu, F.; He, L.; Wang, Y.; Cheng, L.; Chang, L.-T.; Lang, M.; Huang, G.; Kou, X.; Zhou, Y.; Jiang, X.; Chen, Z.; Zou, J.; Shailos, A.; Wang, K. L. *Nat. Nanotechnol.* **2011**, *6* (4), 216−221.

(14) Steinberg, H.; Laloe, J. B.; Fatemi, V.; Moodera, J. S.; Jarillo-Herrero, P. *Phys. Rev. B* **2011**, *84*, 233101.

(15) Wang, Z.; Lin, T.; Wei, P.; Liu, X.; Dumas, R.; Liu, K.; Shi, J. *Appl. Phys. Lett.* **2010**, *97* (4), 042112−3.

(16) Qu, D.-X.; Hor, Y. S.; Xiong, J.; Cava, R. J.; Ong, N. P. *Science* **2010**, *329* (5993), 821−824.

(17) Ren, Z.; Taskin, A. A.; Sasaki, S.; Segawa, K.; Ando, Y. *Phys. Rev. B* **2010**, *82* (24), 241306.

(18) Taskin, A. A.; Ren, Z.; Sasaki, S.; Segawa, K.; Ando, Y. *Phys. Rev. Lett.* **2011**, *107* (1), 016801.

(19) Kou, X. F.; He, L.; Xiu, F. X.; Lang, M. R.; Liao, Z. M.; Wang, Y.; Fedorov, A. V.; Yu, X. X.; Tang, J. S.; Huang, G.; Jiang, X. W.; Zhu, J. F.; Zou, J.; Wang, K. L. *Appl. Phys. Lett.* **2011**, *98*, 242102.

(20) Grove, A. S. *Physics and Technology of Semiconductor Devices*; Wiley: New York, 1967.

(21) Köhler, H.; Fabbicius, A. *Phys. Status Solidi B* **1975**, *71* (2), 487−496.

(22) Zhang, Y.; He, K.; Chang, C.-Z.; Song, C.-L.; Wang, L.-L.; Chen, X.; Jia, J.-F.; Fang, Z.; Dai, X.; Shan, W.-Y.; Shen, S.-Q.; Niu, Q.; Qi, X.-L.; Zhang, S.-C.; Ma, X.-C.; Xue, Q.-K. *Nat. Phys.* **2010**, *6* (8), 584−588.

(23) Kong, D.; Chen, Y.; Cha, J. J.; Zhang, Q.; Analytis, J. g.; Lai, K.; Liu, Z.; Hong, S. S.; Koski, K. J.; Mo, S.-K.; Hussain, Z.; Fisher, I. R.; Shen, Z.-X.; Cui, Y. *Nat. Nanotechnol.* **2011**, *6* (11), 705−709.

(24) Analytis, J. G.; McDonald, R. D.; Riggs, S. C.; Chu, J.-H.; Boebinger, G. S.; Fisher, I. R. *Nat. Phys.* **2010**, *6* (12), 960−964.

(25) Kulbachinskii, V. A.; Miura, N.; Nakagawa, H.; Arimoto, H.; Ikaida, T.; Lostak, P.; Drasar, C. *Phys. Rev. B* **1999**, *59* (24), 15733.

(26) He, L.; Xiu, F.; Wang, Y.; Fedorov, A. V.; Huang, G.; Kou, X.; Lang, M.; Beyermann, W. P.; Zou, J.; Wang, K. L. *J. Appl. Phys.* **2011**, *109*, 103702.

(27) Brüne, C.; Liu, C. X.; Novik, E. G.; Hankiewicz, E. M.; Buhmann, H.; Chen, Y. L.; Qi, X. L.; Shen, Z. X.; Zhang, S. C.; Molenkamp, L. W. *Phys. Rev. Lett.* **2011**, *106* (12), 126803.

(28) Shoenberg, D. *Magnetic Oscillations in Metals*; Cambridge University Press: Cambridge, 1984.

(29) Eto, K.; Ren, Z.; Taskin, A. A.; Segawa, K.; Ando, Y. *Phys. Rev. B* **2010**, *81* (19), 195309.

(30) Das Sarma, S.; Stern, F. *Phys. Rev. B: Condens. Matter* **1985**, *32* (12), 8442.

(31) Li, Y.-Y.; Wang, G.; Zhu, X.-G.; Liu, M.-H.; Ye, C.; Chen, X.; Wang, Y.-Y.; He, K.; Wang, L.-L.; Ma, X.-C.; Zhang, H.-J.; Dai, X.; Fang, Z.; Xie, X.-C.; Liu, Y.; Qi, X.-L.; Jia, J.-F.; Zhang, S.-C.; Xue, Q.-K. *Adv. Mater.* **2010**, *22* (36), 4002−4007.

(32) Lang, M.; He, l.; Xiu, F.; Yu, X.; Tang, J.; Wang, Y.; Kou, X.; Jiang, W.; Chang, L.-T.; Fan, Y.; Jiang, X.; Wang, K. L. *ACS Nano* **2012**, *6* (1), 295−302.